COMPRESSION FATIGUE FAILURE OF CFRP LAMINATES WITH IMPACT DAMAGE

Nobuhide Uda and Kousei Ono
Department of Aeronautics and Astronautics
Kyushu University, Fukuoka, Japan

Keywords: *Fatigue, Failure, Compression, Impact, Damage, CFRP*

Abstract

The objective of this study is to investigate failure mechanisms of compression fatigue behavior of impact-damaged CFRP laminates. Two kinds of composite materials, UT500/Epoxy and AS4/PEEK, were used to examine the dependence of failure behavior on the material properties such as interlaminar toughness. Impact-induced delaminations in the UT500/Epoxy specimen were relatively larger than those in the AS4/PEEK specimen. The S-N curves for the UT500/Epoxy specimens with impact damage showed a similar tendency to those without impact. And the impact-induced delamination in the UT500/Epoxy specimen grew widthwise to the free edge on the rear side of the specimen during the fatigue test. On the other hand, the AS4/PEEK specimens without impact showed the steeper slope of the S-N curve in comparison with those with impact. The delaminations in the impacted AS4/PEEK specimen never reached the free edge before the fatigue fracture.

1 Introduction

The application of composite materials to aircraft primary structures is increasing due to their light weight and high strength nature. However, the excellent mechanical properties of the composite materials can be significantly reduced by a low velocity impact, such as dropped tools during maintenance and runway stones during taxing. A compression-after-impact (CAI) strength of composite structures, in particular, is seriously reduced, even if impact damage is not detectable by visual inspection. A number of investigations [e.g. 1-5] have been conducted to estimate the sensitivity of the CAI strength to low velocity impact damage. Fatigue behavior of impacted composite laminates has been studied extensively during the past couple of decades as well [e.g. 6-10]. However, damage growth mechanisms on post-impact fatigue response have not been fully understood and an efficient damage-tolerance methodology of post-impact composite laminates has not been established. The objective of this study is to investigate failure mechanisms of compression fatigue behavior of impact-damaged CFRP laminates. In the paper, two kinds of composite materials were used to examine the dependence of failure behavior on the material properties such as interlaminar toughness. Some of experimental observations obtained by post-impact compression fatigue tests are reported.

2 Experiments

2.1 Specimens

Composite systems used were UT500/Epoxy (Toho Tenax, QU135-197A) and AS4/PEEK (ICI, APC-2). The AS4/PEEK laminate has a comparatively tougher interface than the UT500/Epoxy laminate. The critical strain energy release rates for mode-I fracture of these materials are 0.28 and 1.40 kJ/m^2, respectively. The lay-up sequence was $[+45/0/-45/90]_{ns}$; n=3 for the UT500/Epoxy and n=4 for the AS4/PEEK. The difference in the number of layups for each material gives almost the same nominal specimen thickness of 4 mm because the prepreg thicknesses are 0.19 mm for the UT500/Epoxy and 0.13 mm for the AS4/PEEK. Specimens of dimensions with 135 mm long by 50 mm wide were cut from 300 × 300 mm panels. The width of unimpacted specimens was reduced to 35 mm taking account of the loading capacity 100 kN of the fatigue testing machine Instron 8501.
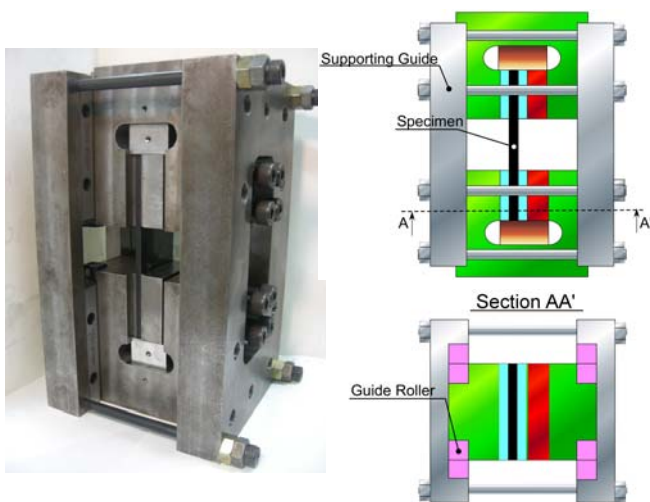
2.2 Impact Tests

Impact tests were performed using a drop-weight test rig with an impactor having a 12 mm

diameter hemispherical tup. The specimen was clamped between two plates, each with a 35 mm diameter circular window. The impactor was captured on the rebound after impact to prevent secondary strikes. The impactor velocity was measured using a laser displacement sensor. The impact energy was defined as the kinetic energy of the impactor just at the moment of first contact with the specimen. The impact energy is normalized by dividing by the thickness of the specimen. The normalized impact energy level was 0.5 to 2.0 J/mm in this study. The damage area induced by the impact load was measured by using ultrasonic C-scan systems with a pulse-echo method, Canon M-500A and GNES G-Scan 6AX500.

2.3 Static and Fatigue Tests

Static compression tests and compression fatigue tests were conducted in the servo-hydraulic testing machine with an end-loading fixture as shown in Fig. 1, which was built based on Shimokawa's work [11]. The specimen was placed in the fixture without tabs and was tightly clamped with binding grips. This fixture does not have an anti-buckling device as prescribed by ASTM D 695, but prevents an out-of-plane direction moving of the specimen by a pair of supporting guides for the whole of the fixture. The compression load is applied through end-sections of the specimen with the binding grips. A gage length of 35 mm for the compression specimen was chosen to prevent global buckling.

The compression-compression fatigue tests were carried out at 1 Hz with constant-amplitude sinusoidal loading, under ambient laboratory conditions. The maximum compressive stress of the cyclic loading was chosen to be 66% to 98% of the ultimate static strength or the residual static strength for the unimpacted and impacted specimens. The minimum compressive stress during fatigue was fixed at 2.5 MPa.

In some cases monitoring damage progression during fatigue was done periodically using the ultrasonic inspection systems to assess a change of the damaged area as a function of the number of load cycles. Some tests were interrupted prior to catastrophic failure in order to reveal the extent of severe damage in the specimen using sectioning technique and microscopic examination.

3 Experimental Results and Discussion

3.1 Impact Damage

The impact-induced damage was mainly delaminations. Figure 2 shows the ultrasonic C-scan images of damage induced in a UT500/Epoxy specimen subjected to 1.91 J/mm impact. The C-scan images in Figs. 2(a) and (b) were taken from the impacted side and the backside of specimen, respectively. The depth of the delamination was indicated using the color gradation shown in Fig. 2. The delaminations are formed in a spiral stair manner in the through-the-thickness direction with each step corresponding to a change in ply orientation. Therefore, the spiral direction is clockwise from the impacted side until the midplane and changed to be counterclockwise below the midplane. The delamination size was measured with an image processing. Figure 3 shows the delamination size at each interface. In Fig. 3, we described the delamination size using the diameter

(a) Overview   (b) Schematic
Fig. 1. Compression test fixture
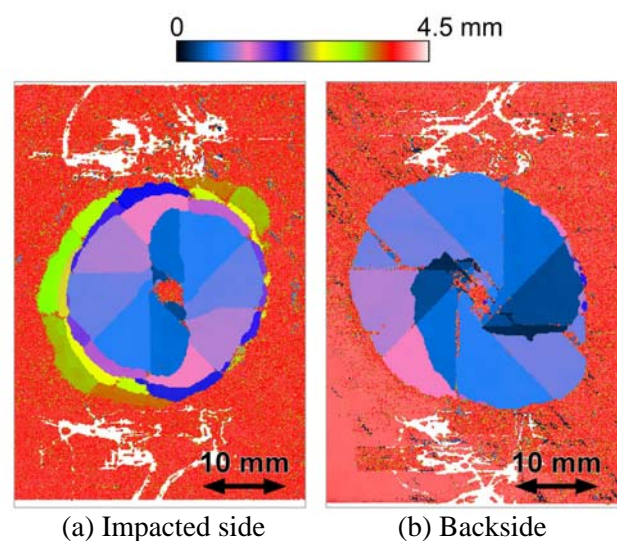
(a) Impacted side   (b) Backside
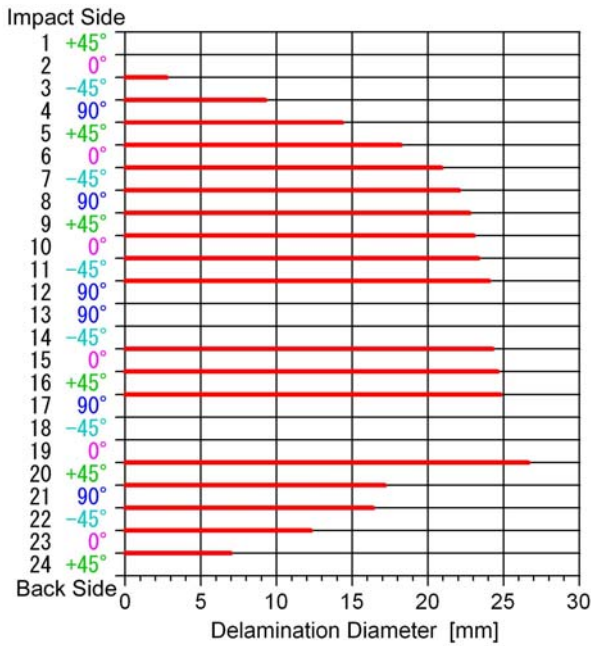Fig. 2. C-scan images of a UT500/Epoxy specimen subjected to 1.91 J/mm impact

Fig. 3. Delamination size at each interface of a UT500/Epoxy specimen subjected to 1.91 J/mm impact

of a hypothetical circle on the assumption that the envelope of the damaged area was circular at each interface. The delamination size increased away from the impacted front face until the interface between the 19th 0-degree ply and the 20th +45-degree ply, and then decreased toward the backside, as shown in Figs. 2 and 3.

In the case of the AS4/PEEK specimen subjected to 1.03 J/mm impact, the delamination area monotonically increased away from the impacted front face towards the back face and three-dimensional envelope of the multiple delaminations created geometrically a truncated cone shape in through-the-thickness direction, as shown in Fig. 4.

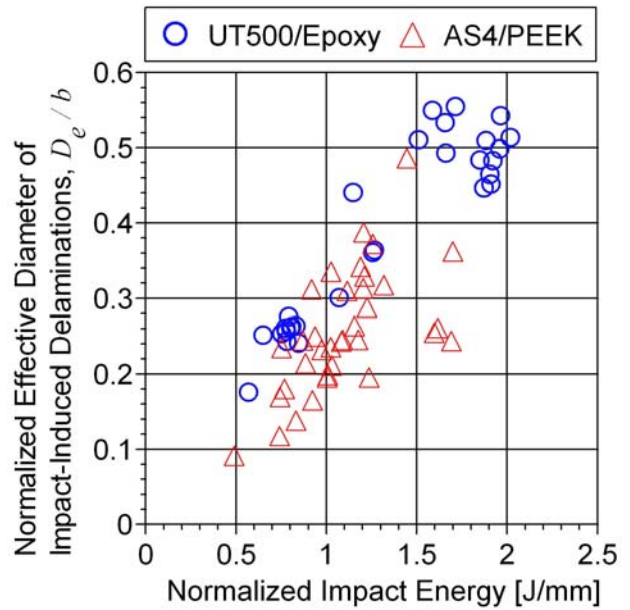Fig. 4. C-scan image of the impacted side for an AS4/PEEK specimen subjected to 1.03 J/mm impact

Fig. 5. Relationships between effective delamination diameter and normalized impact energy

Ishikawa et al. [1] introduced an effective diameter D_e for unified description of CAI strength behavior obtained by various CAI test methods. The effective diameter D_e is defined as the diameter of the hypothetical circle with equivalent area to the delamination geometry. We also adopt the parameter D_e normalized by the width b of the specimen to describe the size of the impact-induced delaminations.

Figure 5 shows relationships between the effective diameter of delaminations D_e and the normalized impact energy. Impacted specimens displayed a large scatter in the delamination diameter. The normalized effective diameter of delaminations of the UT500/Epoxy was relatively larger than that of the AS4/PEEK. This difference in observed damage extents may result from the fracture toughness of each material system.

3.2 CAI Strength

Figure 6 depicts the CAI strength of the laminates. The abscissa is the normalized impact energy. The compressive strengths of the unimpacted specimens were on average 642 MPa for the UT500/Epoxy and 606 MPa for the AS4/PEEK. Figure 7 shows the CAI strength normalized by the ultimate strength of the unimpacted specimens as a function of the normalized effective diameter of delaminations. The CAI strengths of the UT500/Epoxy and AS4/PEEK were reduced to about 40% and 55% of the unimpacted strengths,
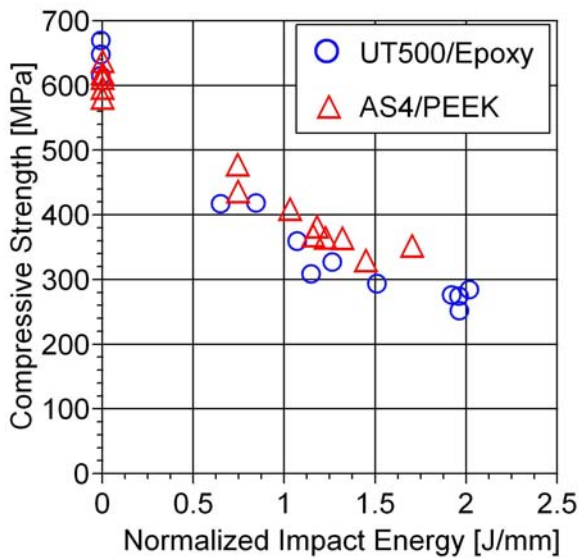
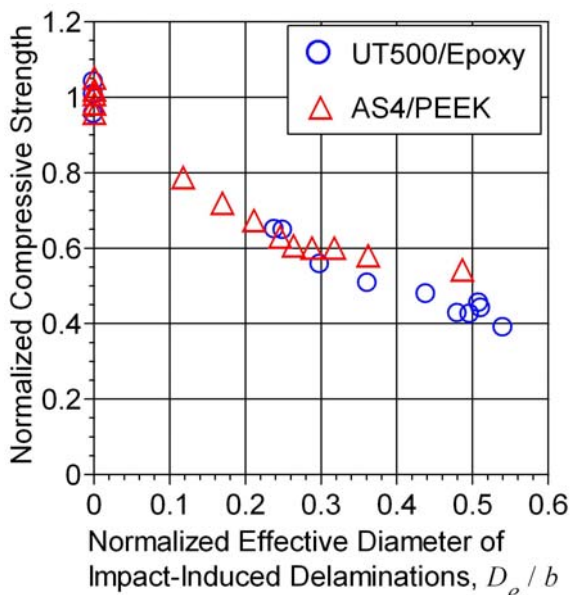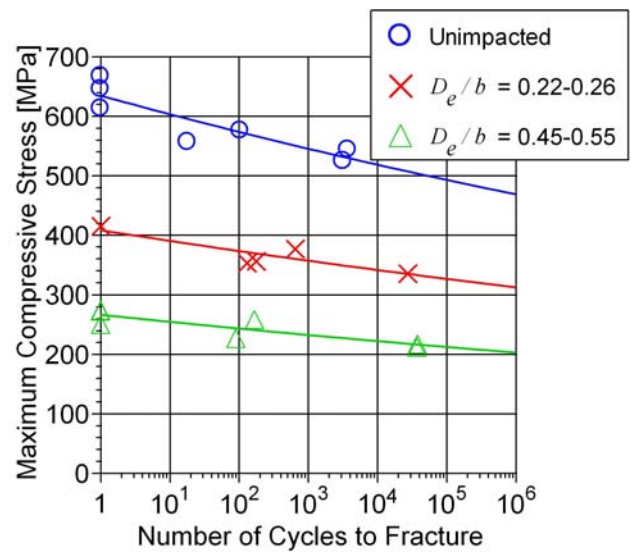Fig. 6. CAI strength as a function of normalized impact energy

(a) UT500/Epoxy laminates

Fig. 7. Normalized CAI strength as a function of normalized effective diameter of delaminations

(b) AS4/PEEK laminates

Fig. 8. S-N curves sorted by the size of the effective delamination diameter

respectively. It was obvious that a tougher composite specimen offered better CAI strength.
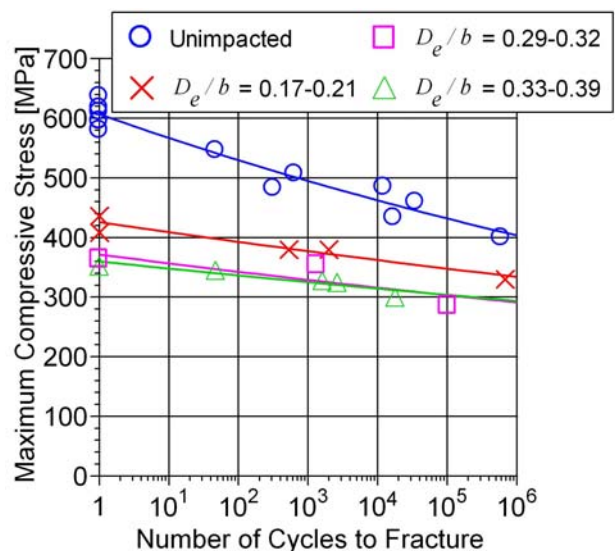
3.3 Post-Impact Compression Fatigue Behavior

3.3.1 S-N curves

Post-impact fatigue test data were processed in the form of relationships between maximum compressive stress and number of cycles to fracture (S-N curves). Figures 8(a) and (b) are depicted using the compression fatigue test data of the specimens sorted into a few groups by the size of the effective delamination diameter. The results of the

UT500/Epoxy and AS4/PEEK are plotted in Figs. 8(a) and (b), respectively. The S-N relationships for the unimpacted specimens are shown by blue circles in Figs. 8. Figures 8(a) and (b) indicate that increasing amounts of the impact damage reduced the compression fatigue performance of the laminate.

In order to clarify the amount of fatigue strength degradation, the S-N curves are plotted using an ordinate normalized by the CAI strengths of the specimens with the same damage size, as shown in Figs. 9(a) and (b). In the case of the UT500/Epoxy, the specimens with impact damage showed similar decrease rate in the fatigue strength
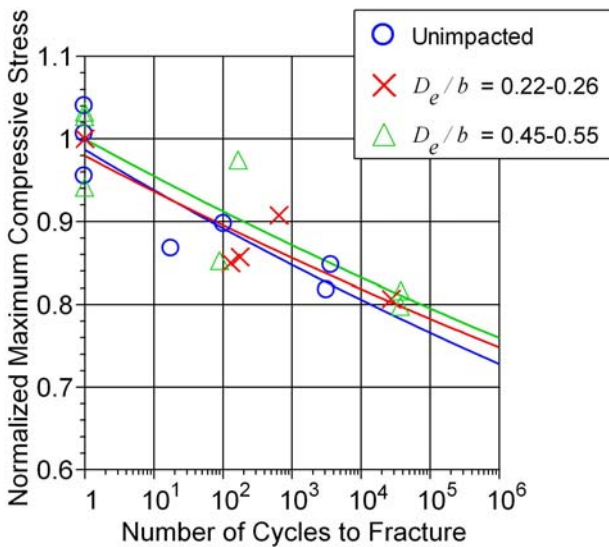
(a) UT500/Epoxy laminates
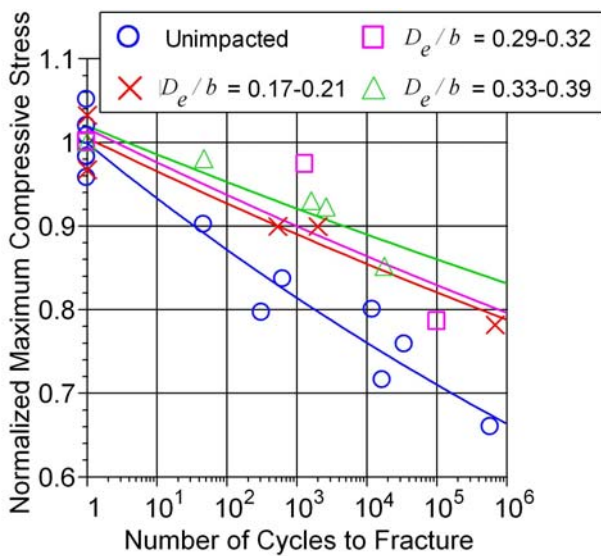
(b) AS4/PEEK laminates

Fig. 9. Normalized maximum compressive stress as a function of cycle number to fracture

to those without impact. On the other hand, the AS4/PEEK specimens without impact showed the steeper slope of the S-N curve in comparison with those with impact.

3.3.2 Specimen deformation during fatigue

In the case of the unimpacted specimens, any large out-of-plane deflection was not observed during fatigue. Figure 10 shows photographs of an unimpacted AS4/PEEK specimen under fatigue loading. The specimen was cyclically subjected to a maximum compressive stress of 507 MPa. The number of cycles to fracture of this specimen was 638. A small delamination of a surface layer at the


(a) N=637   (b) N=638

Fig. 10. Photographs of an unimpacted AS4/PEEK specimen in fatigue
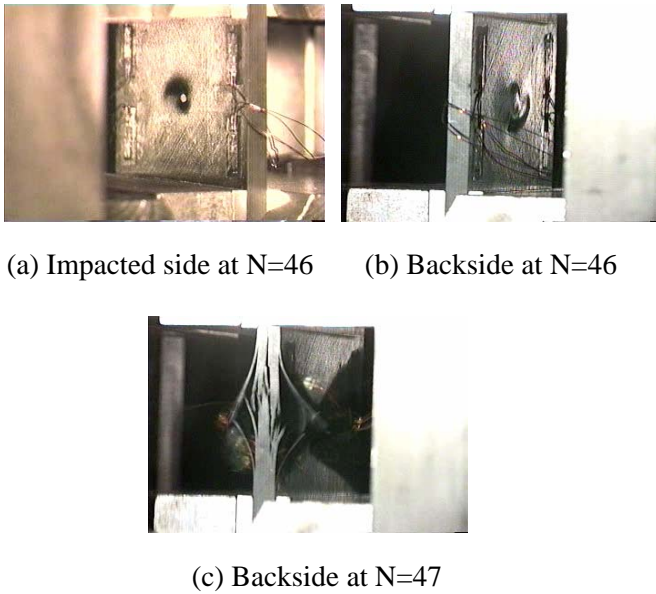(Fatigue life of this specimen was 638.)

free edge was initiated at one cycle before the fracture, as circled with a red in Fig. 10(a). The specimen was abruptly broken during the 638th loading as shown in Fig. 10(b). All of the unimpacted specimens for both the material systems were catastrophically fractured as shown in Fig. 10.

Figure 11 shows photographs of an impacted UT500/Epoxy specimen during fatigue loading. This specimen was subjected to 1.59 J/mm impact that caused the delaminations with $D_e/b = 0.55$, and subsequently cyclically loaded to a maximum compressive stress of 217 MPa. The number of cycles to fracture of this specimen was 37,750. Figure 11(a) represents the delamination extended to the free edge and the back-surface sublaminate was locally deformed in the out-of-plane direction at the 37,700th loading. Fig. 11(b) shows the fractured specimen at the 37,750th loading.

Figure 12 shows photographs of an impacted AS4/PEEK specimen in fatigue. This specimen was subjected to 1.26 J/mm impact and delaminations with $D_e/b = 0.37$ occurred. The maximum compressive stress of this specimen during the fatigue test was 345 MPa. The fatigue life of this
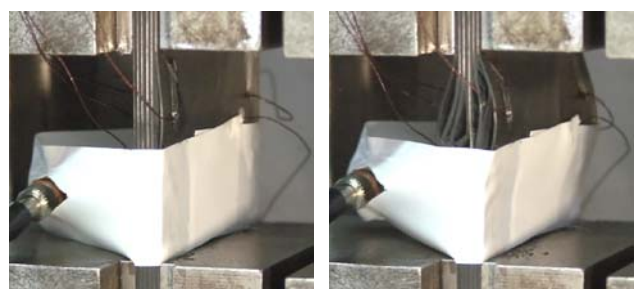

(a) Backside at N=37,700 (b) Backside at N=37,750

Fig. 11. Photographs of an impacted UT500/Epoxy specimen with $D_e/b = 0.55$ in fatigue.
(Fatigue life of this specimen was 37,750.)

(a) Impacted side at N=46   (b) Backside at N=46

(c) Backside at N=47

Fig. 12. Photographs of an impacted AS4/PEEK specimen with D_e/b = 0.37 in fatigue. (Fatigue life of this specimen was 47.)

specimen was 47 load cycles. Figures 12(a) and (b) represent the impacted side and the rear side of the specimen loaded at the 46th cycle, respectively. The impact crater and its vicinity were sunk into the out-of-plane direction and the thin surface layer on the rear side of the specimen was locally buckled as shown in Figs. 12(a) and (b). The specimen was abruptly fractured at the 47th loading as shown in Fig. 12(c).
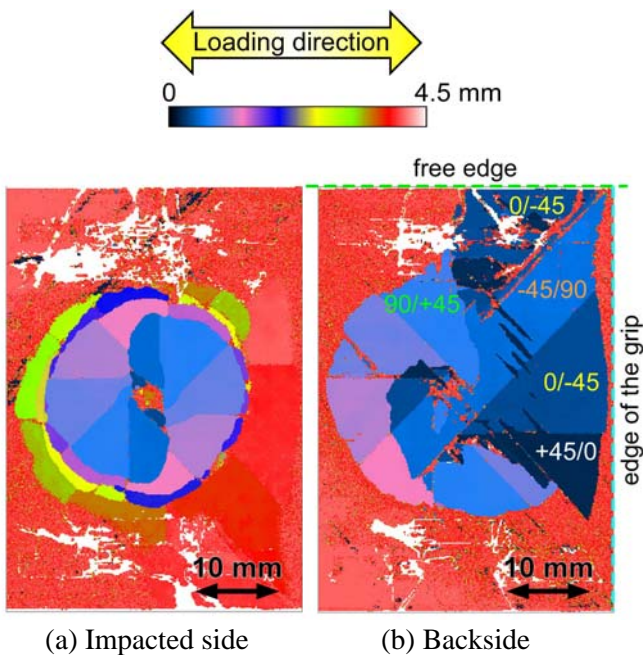
(a) Impacted side   (b) Backside

Fig. 13. C-scan images of the UT500/Epoxy specimen at N=16,468, the impact-induced delaminations of which were shown in Figs. 2 and 3

3.3.3 Damage growth during fatigue

Some specimens were inspected using the pulse echo systems to assess damage progression during fatigue.

Figure 13 shows delamination growth behavior of the UT500/Epoxy specimen, the impact-induced delaminations of which were shown in Figs. 2 and 3. This specimen was subjected to 1.91 J/mm impact, as mentioned before, that caused the delaminations with D_e/b = 0.46, and subsequently cyclically loaded to a maximum compressive stress of 244 MPa. Figure 13 indicates the C-scan images of the specimen just after the 16,468th cyclic loading, when the specimen had not yet been fractured. The loading direction is right and left in Fig. 13. Examination of the C-scan images in Fig. 2 and Fig. 13 reveals that the impact-induced damage grew widthwise to the free edge on the rear side of the specimen during the fatigue test. The delamination between the 22nd -45-degree ply and the 23rd 0-degree ply reached the free edge. And the delaminations on the rear side propagated in the loading direction to the edge of the binding grip.

Figure 14 show the C-scan images of the AS4/PEEK specimen just after the 500th loading, the impact-induced delaminations of which were shown in Fig. 4. This specimen was subjected to 1.03 J/mm impact, as mentioned before, and the delaminations with D_e/b = 0.33 occurred. The maximum compressive stress during fatigue was 327 MPa. Comparing Fig. 14 with Fig. 4, it is obvious that the impact-induced damage on the rear side grew widthwise a little but not lengthwise during

Fig. 14. C-scan image of the impacted side for the AS4/PEEK specimen at N=500, the impact-induced delaminations of which were shown in Fig. 4

(a) Under the edge of   (b) At the edge of the
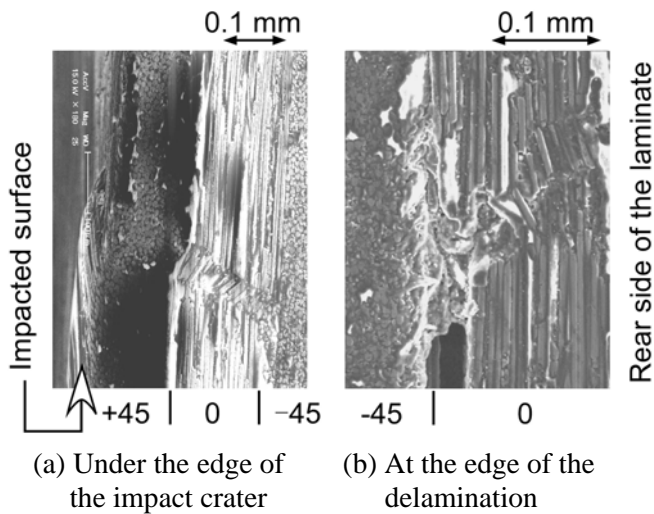   the impact crater   delamination

Fig. 15.   SEM photographs showing kink band occurred at the 0-degree ply in the AS4/PEEK specimen laminate.

fatigue. C-scan image just after the 1,000th loading showed the delamination on the rear side extended widthwise in 2 mm more. However, the delaminations never reached the free edge before the fatigue fracture.

Several post-impact fatigue tests were interrupted in order to inspect an interior damage after measuring a large amount of AE (acoustic emission). The specimens were sectioned in the vicinity of the impact crater using a diamond-impregnated saw, and the cross sections were examined with a scanning electron microscope (SEM). Abrasive papers were used to polish the cross-section so that interior regions of the laminates could be inspected. Figure 15 indicates a kink band observed at the 0-degree ply in the AS4/PEEK specimen during the post-impact fatigue test. Figure 15(a) indicates a kink band observed at the 0-degree ply under the edge of the impact crater. Figure 15(b) shows a kink band caused in the 0-degree ply at the edge of the delamination between the 0-degree ply and the -45-degree ply near the rear surface. The number of loading cycles of the sectioned specimens almost reached the fatigue life on the S-N curve shown in Fig. 8(b). The fiber microbuckling and kinking seem to be intimately related to fatigue fracture.

On the other hand, in the impacted UT500/Epoxy specimens during fatigue, any kink band has not been observed so far.

4 Conclusions

The following findings were obtained through the post-impact compression fatigue tests of UT500/Epoxy and AS4/PEEK.
1. Impact-induced delaminations in the UT500/Epoxy specimen were relatively larger than those in the AS4/PEEK specimen.
2. The CAI strengths of the UT500/Epoxy and AS4/PEEK were reduced to about 40% and 55% of the unimpacted strengths, respectively.
3. Increasing amounts of the impact damage reduced the compression fatigue performance of the laminate.
4. The S-N curves for the UT500/Epoxy specimens with impact damage showed a similar tendency to those without impact. And the impact-induced delamination in the UT500/Epoxy specimen grew widthwise to the free edge on the rear side of the specimen during the fatigue test.
5. The AS4/PEEK specimens without impact showed the steeper slope of the S-N curve in comparison with those with impact. The delaminations in the impacted AS4/PEEK specimen never reached the free edge before the fatigue fracture.
6. Fiber microbuckling and kinking were observed in the 0-degree ply of the AS4/PEEK specimen under post-impact compression fatigue.

Acknowledgements

References

[1] Ishikawa T. and Suemasu H. "Clarification of mechanical behavior in compression after impact (CAI) and open hole compression (OHC) tests for carbon/polymer composites". *Proceedings of the Tenth US-Japan Conference Composites Materials*, Stanford, CA USA, pp.21-32, 2002.

[2] Suemasu H., Osada Y. and Wakabayashi H. "Compressive behavior of composite laminates with different size multiple delaminations", *Proceedings of the ICCM-13*, Beijing, China, ID-1654, 2001.

[3] Davies G.A.O. and Zhang X. "Impact damage prediction in carbon composite structures". *International Journal of Impact Engineering*, Vol.16, pp.149-170, 1995.

[4] Soutis C. and Curtis P.T. "Prediction of the post-impact compressive strength of CFRP laminated

composites". *Composites Science and Technology*, Vol.56, pp.677-684, 1996.

[5] Zhou G. and Rivera L.A. "Investigation for the reduction of in-plane compressive strength in preconditioned thin composite panels". Journal of Composite Materials, Vol. 39, pp.391-422, 2005.

[6] Swanson S.R., Cairns D.S., Guyll M.E. and Johnson D. "Compression fatigue response for carbon fiber with conventional and toughened epoxy matrices with damage". *ASME Journal of Engineering Materials and Technology*, Vol.115, pp.116-121, 1993.

[7] Ding Y.Q., Yan Y. and McIlhagger R. "Effect of impact and fatigue loads on the strength of plain weave carbon-epoxy composites". *Journal of Materials Processing Technology*, Vol.55, pp.58-62, 1995.

[8] Beheshty M.H. and Harris B. "A constant-life model of fatigue behaviour for carbon-fibre composites: The effect of impact damage". *Composites Science and Technology*, Vol.58, pp.9-18, 1998.

[9] Mitrovic M., Hahn H.T., Carman G.P. and Shyprykevich P. "Effect of loading parameters on the fatigue behavior of impact damaged composite laminates". *Composites Science and Technology*, Vol.59, pp.2059-2078, 1999.

[10] Katerelos D.G., Paipetis A. And Kostopoulos V. "A simple model for the prediction of the fatigue delamination growth of impacted composite panels". *Fatigue & Fracture of Engineering Materials & Structures*, Vol.27, pp.911-922, 2004.

[11] Shimokawa T., Hamaguchi Y., Kakuta Y., Katoh H., Sanda T., Mizuno H. and Toi Y. "Effect of isothermal aging on ultimate strength of high-temperature composite materials for SST structures", *Journal of Composite Materials*, Vol.33, 1999, pp.1104-1118.